Influence of point defects injection on the stability of a supersaturated Ga-Si solid solution

Lucia Romano, Alberto M. Piro, and Maria G. Grimaldi
MATIS-INFM and Dipartimento di Fisica e Astronomia, Università di Catania, Via S. Sofia 64, 95123 Catania, Italy

Giorgia M. Lopez and Vincenzo Fiorentini
INFM-SLACS, Sardinian Laboratory for Computational Materials Science, and Department of Physics, University of Cagliari, Italy
(Received 15 July 2004; revised manuscript received 19 January 2005; published 1 April 2005)

The ultrahigh doping levels of Si needed in ultradownscaled electronic devices can be achieved forming supersaturated solid solutions by solid-phase epitaxy. These solutions are, however, unstable upon high-temperature annealing, and electrical deactivation of the impurities exceeding the solid solubility limit occurs. There are indications that deactivation is driven by the interaction of impurities with native (i.e., intrinsic) defects, but the relevant process has not been studied in detail thus far, nor have the defect complexes presumably causing the deactivation been identified. Here we use light-ion beam treatments and Rutherford backscattering analysis combined with first-principles density-functional calculations to investigate the interaction of a specific Group-III acceptor, Ga, with native defects—mostly self-interstitials—generated by irradiation at room temperature, or upon thermal annealing. Monitoring the off-lattice displacement of Ga during He-beam irradiation at room temperature or after high-temperature annealing by channeling analysis, we find a partitioning into substitutional and tetrahedral interstitial Ga populations in the former case, and a partitioning into substitutional and random populations in the latter. Based on *ab initio* calculations and angular-scan Rutherford backscattering spectroscopy, we are able to interpret the results in terms of (a) self-interstitial-assisted enhanced diffusion of Ga, and (b) the subsequent formation of stable Ga-Ga and Ga-Ga-Si complexes. This suggests that deactivation is indeed mediated by native defects (mainly self-interstitials) causing the off-site displacement of the Ga impurity.

DOI: 10.1103/PhysRevB.71.165201 PACS number(s): 61.72.Tt, 61.72.Bb, 61.72.Ji

I. INTRODUCTION

The need to reduce the sheet resistance of the conducting channel of ultradownscaled Si-based devices requires a continuous increase of the active dopant concentration, which, however, is limited by the solid solubility of the dopant species. A route to circumvent this limit is metastable ultrahigh doping as obtained[1–6] by solid-phase-epitaxy (SPE), a low-temperature ($T<600$ °C) treatment by which carrier densities of order 1×10^{21} cm^{-3} have been reached for several dopants in Si.[3] Not unexpectedly, SPE-generated solid solutions are metastable towards dopant precipitation and electrical deactivation upon annealing above typically 600 °C.[7,8]

The mechanisms involved in the deactivation or precipitation of SPE solid solutions have not been investigated so far [although it is known[9–11] that precipitates are not detectable by TEM (trasmission electron microscopy)], nor have even the simplest defect complexes that can actuate—or act as precursors of—deactivation and precipitation ever been experimentally identified. In this paper, we fill this gap, analyzing the deactivation mechanism of the Ga impurity in Si (a choice dictated by the critical solubility of p dopants[3,12] and by previous reports[3,13–16] of SPE-grown active Ga densities of 1.5×10^{20} at/cm^3 even at high T for short annealing times[17]).

Native defects, and especially the Si self interstitial (Si_I) released by end-of-range (EOR) defects[18,19] in self-implant-preamorphized Si, are expected to play a crucial role[20–22] in assisting impurity displacement and de-activation, since stand-alone impurity diffusion at the relevant temperatures would be negligible in defect-free crystalline Si. Here we use ion-beam treatments, Rutherford backscattering spectrometry (RBS), Hall measurements, and first-principles calculations to pinpoint the role of native defects, and identify the relevant impurity-involving complexes they form, or cause to form.

We study the stability of the Ga-Si solution in the 700–900 °C temperature range, finding that electrically inactive Ga complexes involving substitutional Ga atoms are formed during annealing. In addition, we analyze the stability of Ga at room temperature (RT) when an excess of point defects is produced by irradiation with light ions. We observe that upon irradiation at RT a fraction of Ga atoms is displaced from substitutional (Ga_{Si}) to tetrahedral-interstitial (Ga_T) site until a steady state is reached. By first-principles calculations on Ga energetics, diffusion, and complexing in Si, we find that, when coupled to Si_I, Ga is sufficiently mobile at RT to reach other Ga centers during the observation time, and couple to them: for moderate Si_I excess, we predict the formation of a trigonal Ga_{Si}-Ga_T complex as the lowest-energy configuration of Ga, while for strong Si_I excess a Ga_{Si}-Ga_T-Si_I complex is predicted. The computed geometries of these complexes and those inferred by angular-scan RBS and channeling RBS are quite consistent, a result which clearly supports our interpretation.

II. METHODS

The Ga doped Si samples are prepared by implanting $^{69}Ga^+$ at RT into a 550 nm thick Si layer preamorphized by

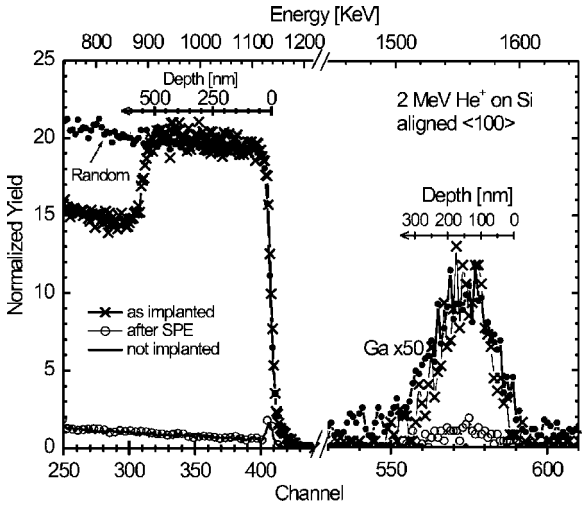

FIG. 1. Energy spectra of a 2 MeV He beam incident on a Ga-implanted (1.3×10^{15} Ga/cm^2) silicon: (●) random; (×, ○, —) ⟨100⟩ channeling. The spectra are relative to: (×) as implanted sample, (○, ●) after annealing at 580 °C for 1 h, (—) not implanted crystal. Ga signal is magnified (×50), the peak concentration is $\sim1\times10^{20}$ Ga/cm^3.

Si implantation at liquid N_2 temperature. The substrate is ⟨100⟩ oriented Czochralski Si, *n* type, $\rho=1.5-4$ Ωcm. The Ga^+ implantation energies are 90 and 160 keV; the fluences are varied in order to obtain a surface region with flat Ga concentration (e.g., 2×10^{14} and 1.1×10^{15} Ga/cm^2 at 90 and 160 keV, respectively, to obtain a maximum Ga concentration of 1×10^{20} at/cm^3). The Ga concentration varies in the range between 0.3 and 4×10^{20} cm^{-3} by scaling the implanted fluences. Samples are annealed in a vacuum furnace ($p\sim10^{-7}$ mbar) at 580 °C for 1 h to crystallize amorphous Si by SPE.

The lattice location of Ga is determined by RBS channeling along different crystal axes (⟨100⟩, ⟨110⟩, ⟨111⟩) using a 2 MeV He^+ beam. To perform the channeling analyses, the beam is first aligned parallel to the selected crystal axis, subsequently intercepted by a shutter while the sample is shifted to start recording the channeling spectrum on a nonirradiated spot.

First-principles gradient-density-functional calculations are performed in 64-site diamond-structure supercells, using the ultrasoft-pseudopotential plane wave method (220 eV cutoff, $4\times4\times4$ k-mesh, Leslie-Gillan correction for charged states) as implemented in the VASP code (see Ref. 23 for more technical details). To avoid artifacts, no symmetry is imposed on any of the systems investigated, and the resulting symmetries indicated in the text are therefore approximate.

III. RESULTS

In Fig. 1 the ⟨100⟩ channeling spectra of a 2 MeV He^+ beam relative to the as implanted and annealed samples are reported along with the random spectrum of the annealed sample. The implantations generated a 550 nm thick amorphous layer. This layer is completely recrystallized by SPE annealing at 580 °C, as certified by the channeling spectrum, identical to that of unimplanted Si, reported in the same figure. No significant diffusion of Ga occurs during SPE, although the large reduction of the channeling yield suggests that most Ga atoms are substitutional in the epitaxial layer after SPE. To check the lattice location of Ga we performed channeling analyses along the main Si axes; the Ga normalized yields ($\chi=A^{Ga}_{all}/A^{Ga}_{random}$ where A^{Ga}_{all} and A^{Ga}_{random} are the areas of the Ga signal in the aligned and random spectra, respectively) are reported in Table I for different Ga concentrations. At low Ga concentration the χ are all close to 10% indicating that ~90% of Ga is substitutional. At a Ga concentration of 4×10^{20} cm^{-3} the channeling yield increases to 50% and the maximum concentration of the substitutional Ga atoms is 2×10^{20} cm^{-3}.

Figure 2 reports the sheet resistance and the carrier surface concentration (measured by Van der Pauw and Hall-effect methods) of the annealed samples as a function of the implanted Ga fluence. The sheet resistance of Ga-doped Si after SPE (filled symbols, Fig. 2(a)) decreases from 500 to 200 Ω/sq as the Ga concentration increases from 3×10^{19} to 2×10^{20} at/cm^3 because of the enhancement of the carrier surface concentration [filled symbols in Fig. 2(b)]. The solid line in Fig. 2(b) marks the carrier concentration expected in case of complete Ga activation; the experimental data are consistent with complete activation, up to a Ga concentration of $\sim2\times10^{20}$ at/cm^3. Above this value the carrier surface concentration saturates. Therefore, the maximum car-

TABLE I. Ga normalized yield for ⟨100⟩, ⟨110⟩, and ⟨111⟩ channeling measured in samples doped with 1×10^{20} and 2×10^{20} Ga/cm^3. The values of χ are measured after SPE and post treatments (none, TA=annealing at 900 °C fro 10 sec, He=irradiation with 4×10^{15} He^+/cm^2). RBS-estimated substitutional fraction (f_{subst}) and Ga concentration ($[Ga]_{subst}$) and the Hall carrier concentration (p) are in units of 10^{20} at/cm^3. Carrier concentration could not be measured after irradiation due to the substrate-doped layer junction leakage.

[Ga] [10^{20} cm^{-3}]	Treatment	$\chi^{\langle100\rangle}$	$\chi^{\langle110\rangle}$	$\chi^{\langle111\rangle}$	f_{subst}	$[Ga]_{subst}$ [10^{20} cm^{-3}]	p [10^{20} cm^{-3}]
1	SPE	0.07	0.12	0.09	0.95	0.95	0.94
2	SPE	0.13	0.14	0.12	0.90	1.80	1.70
1	SPE+TA	0.36	0.36	0.35	0.66	0.66	0.35
2	SPE+TA	0.57	0.58	0.55	0.45	0.90	0.40
1	SPE+He	0.24	0.57	0.24	0.45	0.45	—
2	SPE+He	0.25	0.59	0.23	0.42	0.84	—

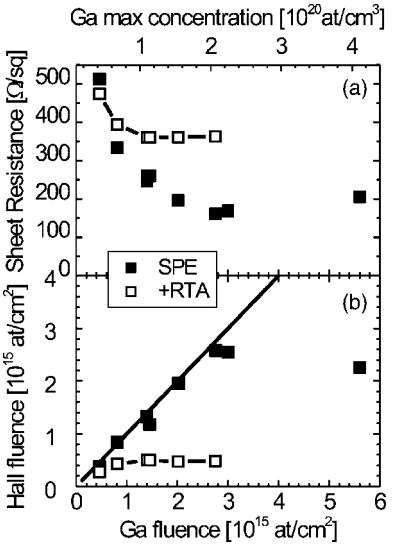

FIG. 2. (a) Sheet resistance as function of the Ga implanted fluence measured on samples after SPE (filled symbols) and after RTA at 900 °C 10 sec (empty symbols). (b) Surface carrier concentration measured by Hall effect as function of the implanted Ga fluence for samples after SPE (filled symbols) and after RTA at 900 °C 10 sec (empty symbols). The solid line indicates the complete activation of the implanted fluence.

rier concentration achieved by SPE is $\sim 2\times 10^{20}$ cm^{-3}, much higher than the Ga solid solubility (4×10^{19} at/cm^3) and in agreement with the substitutional Ga concentration determined by channeling analyses.

The sheet resistance and the carrier concentration after RTA treatments for 10 sec are independent of the annealing temperature in the 700–900 °C range, as reported in Fig. 2 (empty symbols). As expected, the thermal treatment produces the electrical deactivation of Ga exceeding the solubility limit, and the maximum active carrier concentration drops to 4×10^{19} cm^{-3}. The results of the RBS channeling analyses after RTA at 900 °C are reported in Table I. The $\chi_{\min}$ along the different axes increases with respect to the unannealed samples, with about 65% and 45% of the implanted Ga remaining substitutional for Ga concentrations, respectively, of 1×10^{20} and 2×10^{20} at/cm^3. The Ga channeling yield χ increases identically in all the high-symmetry directions, indicating a random location of nonsubstitutional Ga atoms. It should be noted that the concentration of substitutional Ga is always higher than the carrier concentration, which suggests the formation of complexes involving electrically inactive substitutional Ga atoms. However, no agglomerates have been observed in the sample implanted at a concentration of 2×10^{20} at/cm^3 (or lower) by plane-view TEM analyses at 10^6 magnification. This is consistent with results on the deactivation of supersaturated solid Si solutions doped with As[9] or Sb,[10] whereby the formation of electrically inactive complexes involving substitutional dopant atoms, but not visible by TEM, was demostrated. The formation of large agglomerates visible by TEM requires thermal treatments at very high temperatures and/or very high dopant concentration. In particular Ga precipitates have been detected by TEM for a Ga concentration as high as 5×10^{20} Ga/cm^3.[3,15]

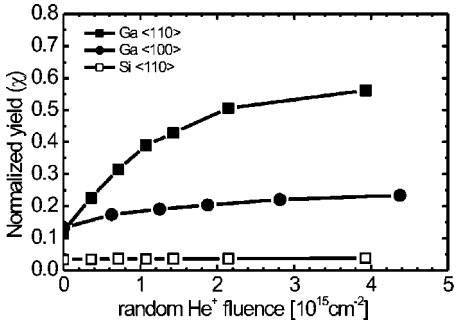

FIG. 3. Normalized yield for ⟨110⟩ and ⟨100⟩ channeling as function of the He$^+$ fluence random incident on Si doped with 1×10^{20} Ga/cm^3.

It is likely that point defects play a relevant role in the formation of the electrically inactive clusters. In fact, a large concentration of Si_I is generated by the dissolution of the EOR defects during annealing[18,19] and, on the other hand, an enhanced impurity diffusion must be invoked to account for complex formation in the experimental conditions. We therefore investigated the role of native defects as described below.

A. Role of point defects

We studied the stability of the Ga-Si solution at RT in the presence of self-interstitials and vacancies generated at a controlled rate by a 2.0 MeV He beam irradiation at random incidence. The beam projected range is about 7 μm, while Ga is confined in a 300 nm thick surface layer, where the density of the point defects generated by elastic collision is very low (due to the dominance of anelastic energy loss). The displaced Ga is measured by channeling analysis as a function of the fluence of the He$^+$ beam randomly incident on the sample. The size of the beam spot is 1 mm^2 and the typical beam current is 50 nA. We take care to ensure good sample-to-holder thermal contact to avoid beam heating effects. A thermocouple placed close to the sample indicated a maximum temperature rise of 20 °C. We find that the Ga displacement rate was independent of the beam current in the 5–100 nA range.

In Fig. 3 the normalized Si yield $\chi_{\min}$ for ⟨110⟩ channeling is reported as function of the He fluence for a sample implanted with 1×10^{20} Ga/cm^3; the yield remained pinned at the initial value of 4%, typical of a defect-free crystal, under irradiation up to a fluence of $\sim 5\times 10^{15}$ cm^{-2}, indicating that no damage is accumulated in the Si lattice. The normalized yield of Ga for ⟨110⟩ and ⟨100⟩ channeling, reported in the same figure, increased monotonically with fluence until saturation occurred after irradiation with $\sim 2\times 10^{15}$He/cm^2. Considering that the He fluence for each channeling analysis is 1×10^{16} cm^{-2} and assuming the off-lattice displacement produced by the impinging beam to scale as the backscattering yield, we estimate that each channeling analysis is equivalent to a fluence of 4×10^{14} He/cm^2 randomly incident on the sample. Therefore, the effective fluence at the saturation is close to $\sim 4\times 10^{15}$ He/cm^2. Irradiation with He beam produces an off-lattice displacement of Ga, and the

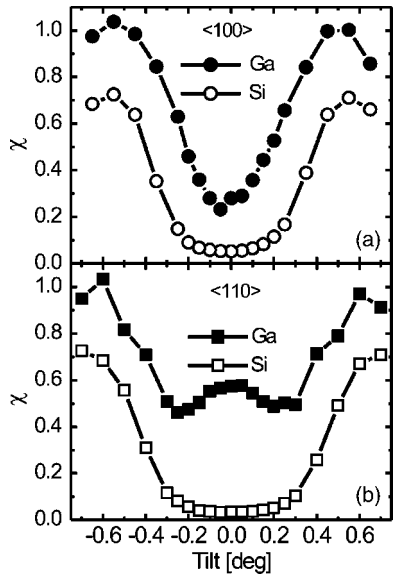

FIG. 4. Angular scans about (a) ⟨100⟩ and (b) ⟨110⟩ axes along the (100) plane.

yield increase is more pronounced for ⟨110⟩ with respect to ⟨100⟩ channeling, indicating a non-random displacement of Ga.

The normalized yield after saturation is reported in Table I for 1 and 2×10^{20} Ga/cm^3 implanted samples. In both cases the χ's for ⟨100⟩ and ⟨111⟩ are rather similar, but smaller than for ⟨110⟩ channeling. This could indicate that a fraction of the Ga atoms occupy tetrahedral interstitial site T, which is visible along the ⟨110⟩ and shadowed by the Si lattice along the ⟨100⟩ and ⟨111⟩ axes.[24–27] Additional information on the Ga location can be extracted from angular scans along the main axes. In Fig. 4 we report the angular scans about the ⟨100⟩ (Fig. 4(a)) and ⟨110⟩ (Fig. 4(b)) axes performed along the (100) plane in the sample implanted with 1×10^{20} Ga/cm^3 and irradiated with He at a fluence above the saturation. A flux peaking typical of the detected atom being located at a T site, is visible in the ⟨110⟩ scan. Along the ⟨100⟩ channel the χ of Ga is definitively lower with respect to the ⟨110⟩, and only a small displacement toward the inside of the channel can be inferred. While the precise determination of the substitutional, random and interstitial Ga fractions requires a detailed flux calculation inside the channels,[28] we can estimate that, at saturation, about 25% of Ga is random displaced, 45% is substitutional, and 30% occupies T sites.

B. Discussion

A simple model of our observations is that during irradiation a substitutional Ga atom leaves its site and diffuses until binding with another Ga atom to form low energy complexes. Below we discuss the hypotheses that *a*) the Ga displacement is mediated by interaction with Si_I generated by the He beam, completing progressively as the Si_I population increases, and *b*) the dominant complex is a Ga_T-Ga_{Si} pair. Preliminarily, we note the following: the preference of Ga for Si_I-assisted over vacancy-assisted diffusion was demonstrated earlier on,[29] and is confirmed by our own calculations;[23] integrating the Si_I concentration profile (calculated by SRIM)[30] in the 300-nm Ga-containing surface region we estimated that ~1 Si_I/ion is generated by the beam, so that at saturation ($\sim4\times10^{15}$ He/cm^2) the Si_I density in that region is comparable to the implanted Ga fluence; in addition the direct knock-on probability of Ga by the incoming ions is negligible due to the low Ga concentration, and the local temperature rise due to electronic excitation cannot account for diffusion over the 2-nm mean distance between Ga atoms (the thermal regime in a collision cascade lasts less than a nanosecond, hence diffusion over 2 nm would require a diffusion coefficient of $\sim5\times10^{-5}$ cm^2/sec, several orders of magnitude higher than that of Ga at the Si melting point).

In our first-principles calculations (see also Ref. 23) we find that, in analogy to boron, Ga_{Si} binds a Si_I into a Ga_{Si}-Si_I trigonal complex, gaining 0.9 eV in the process. This complex transforms (with a 0.5 eV energy gain) into Ga_T, which migrates (via the transient formation of the Ga_{Si}-Si_I complex,[23] diffusion step length $\sim0.4-0.5$ nm) with a jump rate of 0.15 sec^{-1} at room temperature, resulting from the calculated[23] migration barrier 0.8 eV and an assumed attempt frequency of 10 THz. Given the high Ga density (average Ga-Ga distance ~2 nm), this migration rate—albeit low—is sufficient to cause within the observation time (Ga_T needs an average of 5–10 jumps, or 30–60 sec, to reach a Ga_{Si}) the formation of a further complex: we find that the migrating Ga_T binds with a Ga_{Si} with a 0.6 eV gain, forming a trigonal Ga_{Si}-Ga_T complex. Upon formation of this complex, the diffusion-driving Si_I is annihilated, as one Ga remains interstitial. The same calculation indicates that the Ga_{Si}-Ga_T complex is electrically neutral, so that *both* the participating Ga atoms are electrically deactivated. Note that self-interstitials, which are donors (double, according to theory, e.g., Ref. 23), compensate the Ga acceptors even before the latter are displaced off-site or clustered. As a result, Ga-Si complexes and self-interstitials migrate in their neutral charge state, which is important because their diffusivity in the positively-charged configuration (typical of *p*-type conditions) would be small at room temperature (e.g., the migration barrier for Si_I is 1.2 eV in the 2+ state vs 0.3 eV in the neutral state, respectively).[23] In summary, first-principles results definitely support the interpretation of RT RBS results as being due to Ga_{Si}-Ga_T complexing (driven by self-interstitial-assisted enhanced diffusion) in the presence of a moderate excess of Si_I. The energetics of the whole cascade of events is summarized in Fig. 5 (including the three-body Ga-Ga-Si_I complex discussed next).

Assuming now the Si_I super-saturation to exceed significantly the impurity density (as in the case of high-temperature annealing with release from EOR defects), one expects further channels, such as, e.g., Ga-Ga-Si clustering, to come into play. Further calculations enabled us to identify a Ga-Ga-Si_I complex bound by about 1 eV compared to a Ga_{Si}-Ga_T pair [see Fig. 6(a)] and a remote Si_I. This complex is depicted in Fig. 6(b). The Ga atoms are not placed at sites of high symmetry, so that Ga in this complex should give rise to a "random" RBS signal. Of course many variants of complexes of this sort can exist. In the RT experiment, whereby the excess of Si_I is controlled at a level near to the Ga den-

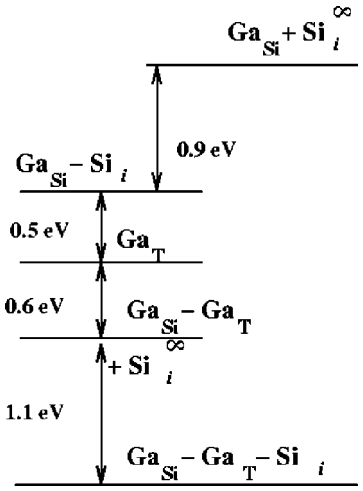

FIG. 5. Schematic energetics of the Ga-Si complexes cascade generated by one Ga and one Si_i originally far apart. As indicated, the bottom step requires a *second* remote Si_i per center.

sity, Ga-Ga-Si clustering (whereof our complex is but the simplest case) causes a random component accounting for only a limited fraction of the displaced Ga. In the high-temperature annealing case, instead, it provides channels for the decay of the Ga-Si solid solution into random Ga complexes. This is consistent with the Ga random component observed after annealing the supersaturated solutions.

In conclusion our experiments indicate the formation of Ga complexes involving substitutional and random displaced Ga during deactivation of supersaturated Ga-Si solid solutions by thermal treatments, while at RT the Ga_{Si}-Ga_T couple is formed in presence of an excess of point defects. *Ab initio* calculations provide a picture consistent with experiments, suggesting that out-of-equilibrium Si_I cause an enhanced diffusion of Ga_{Si} in the form of a Ga_{Si}-Si_I pair, eventually leading to the formation of the more stable Ga_{Si}-Ga_T pair. As the Si_I concentration greatly exceeds the dopant concentration, the formation of Ga_{Si}-Ga_T-Si_I complexes is predicted, leading to disordering and precipitation.

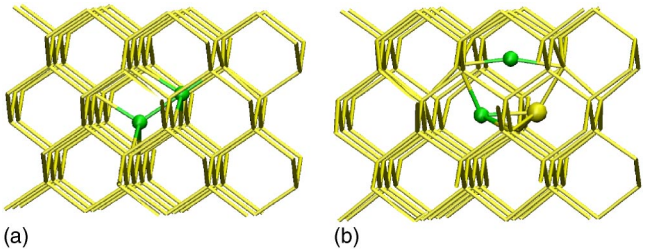

FIG. 6. (Color online) Ground-state configuration of the Ga_T-Ga_{Si} (a) and Ga-Ga-Si_i complexes in Si. Refer to Fig. 5 and text for the energetics.

ACKNOWLEDGMENTS

The authors thank Salvo Tatì for his assistance with the 3.5 MeV Singletron accelerator for RBS analyses. GML and VF thank C. Melis for assistance in the early stages of this project. This work has been partially supported by the Italian Ministry of University and Research under the PRIN-2002 project *Study of the high doping regime in shallow Si and Si alloy layers*, and by INFM Supercomputing Initiative.

[1] P. Blood, W. L. Brown, and G. L. Miller, J. Appl. Phys. **50**, 173 (1979).
[2] G. L. Olson and J. A. Roth, Mater. Sci. Rep. **3**, 1 (1988).
[3] J. Narayan, O. W. Holland, and B. R. Appleton, J. Vac. Sci. Technol. B **1**, 871 (1983).
[4] J. Narayan and O. W. Holland, Appl. Phys. Lett. **41**, 239 (1982).
[5] J. S. Williams, in *Surface Modification and Alloying by Laser, Ion and Electron Beams*, edited by J. M. Poate, G. Foti, and D. C. Jacobson (Plenum Press, New York, 1983), p. 133.
[6] C. W. White, B. R. Appleton, and S. R. Wilson, in *Laser Annealing of Semiconductors*, edited by J. M. Poate and J. W. Mayer (Academic Press, New York, 1982), p. 111.
[7] E. V. Thomsen, O. Hansen, K. H. Petersen, J. L. Hansen, S. Y. Shiryaev, and A. N. Larsen, J. Vac. Sci. Technol. B **12**, 3016 (1994).
[8] C. P. Parry, T. E. Whall, and E. H. C. Parker, J. Appl. Phys. **82**, 4990 (1997).
[9] A. Parisini, A. Bourret, A. Armigliato, M. Servidori, S. Solmi, R. Fabbri, J. R. Regnard, and J. L. Allain, J. Appl. Phys. **67**, 2320 (1990).
[10] Y. Takamura, A. F. Marshall, A. Mehta, J. Arthur, P. B. Griffin, J. D. Plummer, and J. R. Patel, J. Appl. Phys. **95**, 3968 (2004).
[11] G. Glass, H. Kim, P. Desjardins, N. Taylor, T. Spila, Q. Lu, and J. E. Greene, Phys. Rev. B **61**, 7628 (2000).
[12] T. B. Massalski, *Binary Alloy phase Diagrams* (American Society for Metals, Metals Park, OH, 1986).
[13] H. Gnaser, C. Kallmayer, and H. Oechsner, J. Vac. Sci. Technol. B **13**, 19 (1995).
[14] T. Ishitani, H. Koike, T. Yaguchi, and T. Kamino, J. Vac. Sci. Technol. B **16**, 1907 (1998).
[15] Y. Shiryaev, A. N. Larsen, and M. Deicher, J. Appl. Phys. **72**, 410 (1992).
[16] A. Casel, H. Jorke, E. Kasper, and H. Kibbel, Appl. Phys. Lett. **48**, 922 (1986).
[17] J. Matsuo, I. Kato, H. Hoire, N. Nakayama, and H. Ishikawa, Appl. Phys. Lett. **51**, 2037 (1987).
[18] S. Mades, in *Ion implantation: Science and Technology*, edited by J. F. Ziegler (Academic Press, Orlando, 1984), p. 109.
[19] E. Rimini, *Ion Implantation: Basics to Device Fabrication* (Kluwer, Dordrecht, 1995), p. 175.
[20] G. D. Watkins, Chin. J. Phys. (Taipei) **15**, 92 (1977).
[21] H. Bracht, MRS Bull. **25**, 22 (2000).
[22] E. Napolitani, A. Coati, D. De Salvador, A. Carnera, S. Mirabella, S. Scalese, and F. Priolo, Appl. Phys. Lett. **79**, 4145 (2001).
[23] C. Melis, G. M. Lopez, and V. Fiorentini, Appl. Phys. Lett. **85**, 4902 (2004); see also G. M. Lopez and V. Fiorentini, Phys. Rev. B **69**, 155206 (2004).
[24] B. R. Appleton and G. Foti, in *Ion Beam Handbook for Material*

Analysis, edited by J. W. Mayer and E. Rimini (Academic Press, New York, 1977), p. 91.
[25] J. A. Davies, in *Channeling Theory, Observation and Application*, edited by D. V. Morgan (John Wiley & Sons, New York, 1973), p. 391.
[26] L. Eriksson, J. A. Davies, and N. G. E. Johannsson, J. W. Mayer, J. Appl. Phys. **40**, 842 (1969).
[27] L. W. Wigger and F. W. Saris, Nucl. Instrum. Methods **149**, 399 (1978).
[28] M. L. Swanson, in *Handbook of Modern Ion Beam Materials Analysis*, edited by J. R. Tesmer and M. Nastasi (Materials Research Society, Pittsburgh, 1995), p. 274.
[29] P. Fahey, S. S. Iyer, and G. J. Scilla, Appl. Phys. Lett. **54**, 843 (1989).
[30] J. F. Ziegler, J. P. Biresack, and U. Littmark, *The Stopping and the Range of Ions in Solids* (Pergamon, New York, 1985); http://www.srim.org